SM HIGGS PROPERTIES AND RARE DECAYS IN ATLAS*

Marc Escalier

on behalf of the ATLAS Collaboration

IJCLab, PHE department
15 Rue Georges Clemenceau, 91400 Orsay, France

Received 12 February 2025, accepted 13 April 2025, published online 26 June 2025

With the LHC full Run 2 *pp* collision dataset collected at 13 TeV, very precise measurements of Higgs boson properties and its interactions can be performed, shedding light on the electroweak symmetry-breaking mechanism. This contribution presents measurements performed using the Run 2 dataset, as well as first results using the Run 3 *pp* collision dataset collected since 2022 at 13.6 TeV. Measurements of the Higgs boson properties by the ATLAS experiment in various decay channels are shown, including its production cross sections, simplified template cross sections, mass, width, differential and fiducial cross sections, as well as their combination and interpretations. Specific scenarios of physics beyond the Standard Model are tested, as well as a generic extension in the framework of the Standard Model Effective Field Theory. The paper also presents the latest HH searches, which are sensitive to the Higgs boson self-coupling. Results are shown in terms of sensitivity to the SM HH production and limits on the Higgs boson self-coupling.

DOI:10.5506/APhysPolBSupp.18.5-A9

1. Introduction

These proceedings review the recent results of the ATLAS Collaboration [1] on the Higgs sector, with respect to the previous edition of this conference. The simple Higgs boson (also called the single Higgs boson) production results are shown for di-bosons, di-fermions, and some exotic decays, mainly using Run 2 of the LHC datasets at the center-of-mass energy of $\sqrt{s} = 13$ TeV, but also for a partial dataset of Run 3 at $\sqrt{s} = 13.6$ TeV. Then, the results on double- and triple-Higgs boson production are also presented.

* Presented at the 31st Cracow Epiphany Conference on the *Recent LHC Results*, Kraków, Poland, 13–17 January, 2025.

2. Single-Higgs boson production

As opposite to measuring the Higgs boson's decay width directly from rates for various hypotheses, which suffers from the limited detector resolution, thus providing a sensitivity at the GeV level, an indirect approach exhibits much higher sensitivity. In this scenario, by considering the di-Z final state [2], if one introduces the Higgs boson effective couplings in production ($g_{\text{prod}}(\widehat{s})$) and decay ($g_{\text{decay}}(\widehat{s})$) as a function of the Higgs boson virtuality $\widehat{s}$, the differential cross section $\frac{\mathrm{d}\sigma^{H\to ZZ}}{\mathrm{d}m^2_{ZZ}} \propto \frac{g^2_{\text{prod}}(\widehat{s})g^2_{\text{decay}}(\widehat{s})}{(m^2_{ZZ}-m^2_H)^2+m^2_H\Gamma^2_H}$ of the Higgs boson production presents a dependence on the Higgs boson's width in the on-shell region close to a mass of 125 GeV. The degeneracy between the parts related to the coupling and total Higgs boson's width can be raised by measuring this channel in the off-shell region. For both the gluon- and quark-initiated states, the various processes of signal, background, interference between these two and non-interfering background are considered. They present a unique scaling of the cross section with the effective couplings to gluons and vector bosons. The selection requires the Higgs boson to be off-shell. Fourteen observables are used to describe the events, and a preselection cut is applied based on the output of a neural network trained with these observables. From the 14 observables, a novel method the so-called Neural Simulation-Based Inference (NSBI) [3–6] is used to construct the per-event likelihood ratio between the probability density of a given process (considering signal, background, interfering, and non-interfering backgrounds for both gluon- and quark-initiated states) and a reference process, improving sensitivity with respect to a histogram-based discriminant variable approach (figure 1) and to previous analysis [7]. The measurement is combined with

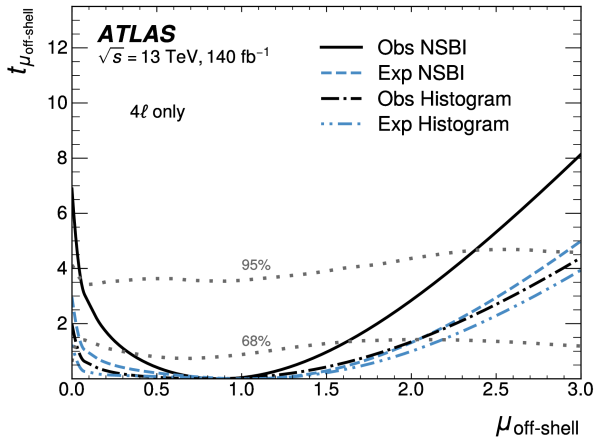

Fig. 1. Comparison of the test statistic distribution between the NSBI technique [2] and from a historical histogram based on a single final discriminant variable.

the off-shell 2 leptons plus 2 neutrinos channel, establishing evidence for the off-shell production of the Higgs boson with an observed significance of 3.7σ. These are further combined with the on-shell $H \to ZZ \to 4l$ channel, allowing to measure an observed (resp. expected) total Higgs boson's width of $\Gamma_H = 4.3^{+2.7}_{-1.9}$ MeV ($\Gamma_H = 4.1^{+3.5}_{-3.4}$ MeV).

The measurements on VH production with $H \to bb$, $H \to cc$ channels [8] have been improved with respect to the previous analyses [9–11], in particular with an improved flavour tagging algorithm and a re-optimisation of multivariate discriminants. The main ingredients of the complex selection include corrections to the b- or c-jets to take into account their semileptonic decays and different energy response with respect to light jets, improving the Higgs boson mass resolution by up to 40% depending on the category. The flavour tagging uses the so-called DL1r neural network, with the 70% and 45% efficiency working points, respectively, for the b- and c-jets. Categories are introduced to distinguish various decays of the vector boson, multiplicities of b-, c-, and light-jets, separating resolved and boosted regimes ($p_{\mathrm{T}}^{V} \gtrless 400$ GeV) for the bb final state. Control regions are used to estimate the large multijet background. Boosted Decisions Trees (BDT) are used as final discriminant variables. The $WH(\to bb)$ process is observed for the first time, with a significance of 5.3σ. In the absence of a significant signal, a 95% C.L. limit of $11.5 \times$ SM is derived for $VH(\to cc)$. By parametrising the signals with the so-called kappa-framework [12, 13], introducing Higgs boson coupling strength modifiers κ, the ratio κ_c/κ_b is probed, allowing us to remove the degree of freedom from assumptions on the Higgs boson's width. The 95% C.L. observed (resp. expected) limit on this ratio is $3.6 \times$ SM ($3.5 \times$ SM), in agreement with the non-universality of Hqq Yukawa coupling. Using reconstructed categories mirroring the corresponding truth-level regions, so-called STXS [13] (Simplified Template Cross Sections), which correspond to cross-section measurements in the fine granularity kinematic regions for various production processes, are measured separately for WH and ZH for various bins of transverse momentum of the vector boson. Results are in agreement with the Standard Model (SM) expectation, and dominated by statistical uncertainty. The analysis is validated by a search for a standard candle di-boson VZ, $Z \to bb, cc$, observed with more than 5σ with signal strength in very good agreement with the SM.

The ttH, $H \to bb$ [14] is also probed. It presents a complex final state with the presence of leptons, jets including b-tagged ones. Categories are used, taking into account the multiplicity of lepton, jets, and b-jets. The 1-lepton category is further splitted into resolved and boosted categories for the b-jets coming from the Higgs boson candidate. A multiclass neural network defines the signal region and control region. A second neural network allows to pair the b-jets to those coming from the Higgs boson candidate

and top decays. This allows us to reconstruct the transverse momentum of the Higgs boson used for STXS. The signal is extracted with an observed (resp. expected) significance of 4.6σ (5.4σ). Both the inclusive and STXS-measured cross sections are compatible with the prediction from the SM. This analysis is the most precise ttH cross-section measurement in a single decay channel, inclusively and in each bin of the Higgs boson transverse momentum.

The $H \to \tau\tau$ channel has been measured as differential cross sections [15] in the gluon fusion, vector-boson fusion (VBF), VH, and ttH production modes, using the three possible final states: hadronic–hadronic, leptonic–hadronic, and leptonic–leptonic, where the latter requests electron and muon in order to suppress the Z background. The statistical measurement is made from a likelihood fit on the di-tau invariant mass estimated from the Missing Mass Calculator [16] (MMC) in order to take into account the neutrinos contributions. To have sensitivity for the various bins of STXS, a categorisation is developed, separating VBF, $tt(0l)H$, $V(\text{had})H$, ggF boosted ($p_{\text{T}}^{H} > 100$ GeV), with a subsplitting by kinematic and output of BDT. For the inclusive level and granularities of production modes and STXS, the cross-sections measurements are in excellent agreement with the prediction from the SM. This is the first VBF measurement in the higher-p_{T}^{H} STXS bin and the most precise for the lower ones. The differential cross section is also extracted explicitly in the VBF fiducial region after unfolding for detector effects and efficiencies, for various kinematic variables including the signed azimuthal separation between the two jets, which allows us to probe CP-odd contributions of the Higgs boson. These unfolded cross sections are interpreted in terms of the Standard Model Effective Field Theory (SMEFT) [17] using the Warsaw basis [18], providing the strongest constraint on the CP-odd Wilson coefficient $c_{H\tilde{W}}$.

The combination of Higgs boson cross sections [19] from $H \to \gamma\gamma$, $H \to ZZ^*$, $H \to \tau\tau$, $H \to WW^*$, $H \to bb$, $H \to Z\gamma$, $H \to \mu\mu$ with the production-level (STXS stage 0) and STXS stage 1.2 granularity has been interpreted in terms of the SMEFT using the Warsaw basis. The cross section times branching ratio are parametrised by introducing in the Lagrangian Wilson coefficients representing strengths of higher-order operators up to dimension 6, constructed from SM operators, suppressed by the beyond-Standard-Model (BSM) energy scale Λ at the relevant power to maintain the dimension 4 of the Lagrangian. Comparing constraints on the Wilson coefficients with the implementation of linear only (in the cross section) or linear+quadratic (in the cross section) allows us to estimate the validity of neglecting dimension 8 terms (suppressed by Λ^4) in the Lagrangian. For the efficiency times acceptance, the parametrisation is not implemented due to the very fine granularity of STXS bins which ensures a weak dependence

with the Wilson coefficients in the restricted kinematic region, but theoretical systematics covers the residual effect. For the decay part of each process, in the 2 bodies decays, it is small enough to be neglected, while for more than 2 bodies decays, a parametrisation is considered. The variation of the shape of the final discriminant with the Wilson coefficient is considered when non-negligible. Despite the important number of channels considered, the limited statistics and correlations among Wilson coefficients drives to probing eigenvectors of the Wilson coefficients instead of the Warsaw basis ones. The results on Wilson coefficients, either by parametrising STXS or alternatively from fiducial differential cross sections in transverse momentum from $H \to \gamma\gamma$ and $H \to ZZ^* \to 4l$ are in very good agreement with the prediction of the SM. Although the granularity in bins is finer for the EFT interpretation from fiducial differential cross sections, the constraints from STXS is more powerful due to the many probed production levels and kinematic regions. The results are also interpreted in terms of 2HDM and MSSM for 8 benchmarks.

Rare channels have been studied. The first inclusive Higgs boson plus charm production [20] has been searched for using the $H \to \gamma\gamma + c$ final state, allowing us to probe the Yukawa Hcc coupling, although it represents only an order of 1% of the whole process. Using the di-photon invariant mass as the final discriminant variable, 95% C.L. observed (resp. expected) upper limits of 10.4 pb (8.6 pb) are derived. The very rare loop-involving $H \to D^*\gamma$

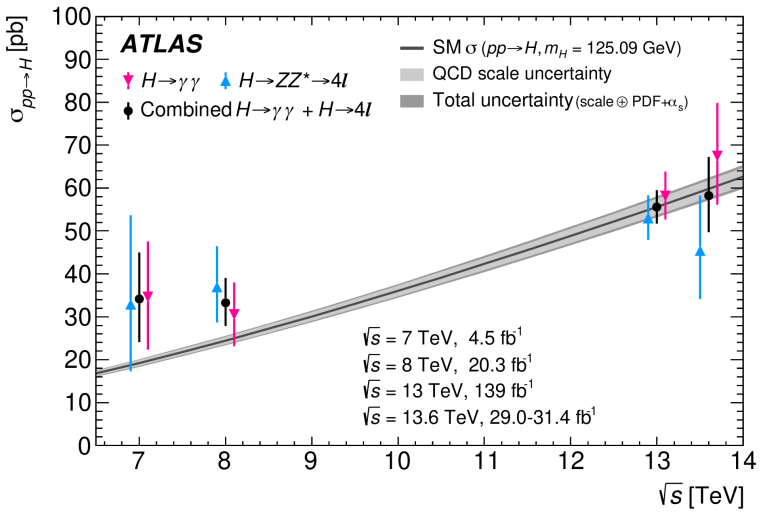

Fig. 2. Evolution of the measured cross sections with the pp centre-of-mass energy [22] and comparison to the expectation from SM. The individual channel results are offset along the x-axis for display purposes.

channel [21] was studied with the $D^* \to D^0\pi^0, D^0\gamma$, $D^0 \to K^-\pi^+$ decays probing BSM by introducing the flavour-violating coupling with a theoretical branching ratio of 7×10^{-27}. Using the 3 bodies $K\pi\gamma$ invariant mass, 95% observed (resp. expected) upper limits of 1.0×10^{-3} (1.2×10^{-3}) are derived. This is the first limit on this decay.

ATLAS has already started to analyse the Higgs sector with the Run 3 dataset [22] at a higher energy in the center-of-mass energy of 13.6 TeV. Using the two precision channels $H \to \gamma\gamma$ and $H \to ZZ^* \to 4l$, fiducial cross sections were measured and extrapolated to full phase space in order to combine them in a total cross section using the ATLAS+CMS Run 1 combined measured mass $m_H = 125.09$ GeV. The result is in excellent agreement with the prediction from the SM and the energy dependence (figure 2) of the cross section, taking into account the previous measurements at 7, 8, and 13 TeV.

3. Double- and triple-Higgs boson production

Previous measurements contribute to the so-called single-Higgs boson production that is the production of a single Higgs boson within a collision of protons. This allows us to infer information on the kinematic Lagrangian of the Higgs boson and the mass term of the Higgs potential. In order to constraint directly the remaining term of the potential, that is the self-coupling of the Higgs boson with himself providing its own mass, one needs to search for the double-Higgs boson production. In the dominant gluon fusion production mode, the double-Higgs boson production has two destructively interfering contributions (figure 3): the triangle diagram where the self-coupling appears, and the box diagram. The secondary ($1/20^{\text{th}}$ of the dominant one) mode is the $VBFHH$ production (figure 4), which allows us to uniquely probe the $VVHH$ vertex. Those couplings are expressed in terms of coupling strength named κ (respectively κ_λ and κ_{2V}).

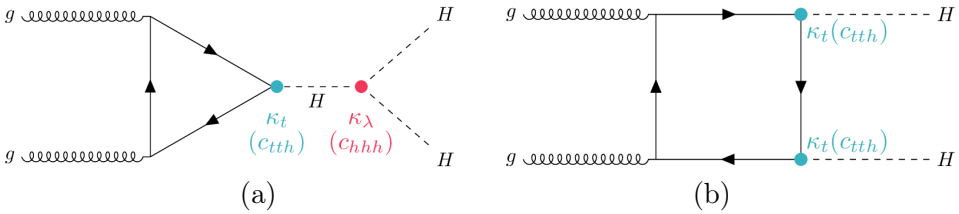

Fig. 3. Leading-order Feynman diagrams [23] showing the production of Higgs boson pairs via the ggF process.

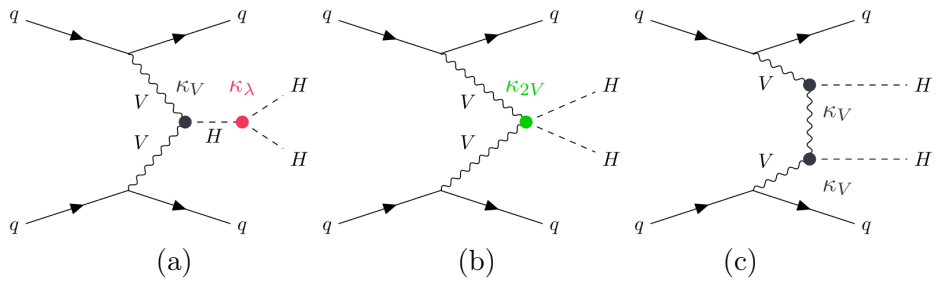

Fig. 4. Leading-order Feynman diagrams [23] showing the production of Higgs boson pairs via the VBF process.

The double-Higgs boson production has been searched for in a wealth of final states and combined [23] to improve sensitivity: *bbbb* (resolved, boosted), $bb\tau\tau$ with at least one hadronic τ, $bb\gamma\gamma$, multilepton (targeting $bbZZ^*$, VV^*VV^*, $VV^*\tau\tau$, $\tau\tau\tau\tau$, $\gamma\gamma VV^*$, $\gamma\gamma\tau\tau$), *bbll*+Missing Transverse Energy (MET), where the two leptons come from $ZZ^*, WW^*, \tau\tau$. The final discriminant variable depends on the channel ($m_{\gamma\gamma}$, reconstructed Higgs boson invariant mass, multivariable quantity, *etc.*). The 95% C.L. observed (resp. expected) limit is $2.9 \times$ SM ($2.4 \times$ SM). The most sensitive channels are $bb\tau\tau$, $bb\gamma\gamma$, *bbbb*. In terms of the observed (resp. expected) significance, this corresponds to 0.4σ (1.0σ). This analysis improves by 17% the sensitivity with respect to the previous results [24], where 13% comes from the improvement of the $bb\tau\tau$, $bb\gamma\gamma$, *bbbb* channels and 4% comes from the introduction of the multilepton and $bbll + \text{MET}$ channels. The 95% confidence observed (resp. expected) intervals are $-1.2 < \kappa_\lambda < 7.2$ ($-1.6 < \kappa_\lambda < 7.2$), where $bb\gamma\gamma$ is the most sensitive and $0.6 < \kappa_{2\text{V}} < 1.5$ ($0.4 < \kappa_{2\text{V}} < 1.6$). This represents the best-expected to date sensitivity on the signal strength and Higgs boson self-coupling. The results are interpreted in HEFT [25, 26] from the 3 most sensitive channels, providing the most stringent constraints to date on c_{gghh} and c_{tthh}.

In the Higgs potential, the Higgs boson self-coupling appears explicitly in two terms: in the term H^3 related to the triple-Higgs boson self-coupling, but also in the term $HHHH$ related to the quadruple-Higgs boson self-coupling. While the SM predicts the same self-coupling term for these two sorts of vertices, Nature may present different ones, thus it is important to measure them. The Higgs boson self-coupling related to the quadruple-Higgs boson vertex could be measured by probing the simultaneous production of three Higgs bosons within the same protons collision. ATLAS has probed searches for this triple-Higgs boson production [27] using the 6 b final state. The pairing algorithm minimises a quantity related to each reconstructed Higgs boson mass over all possible permutations of jet pairs, taking into account energy lost due to detector inefficiencies, neutrinos from b-hadrons

decays, and out-of-cone radiation. The pairing efficiency, that is the fraction of signal events where the reconstructed jets could be matched to the correct truth-level b-quarks from each boson decay is 61%. In order to control the background, control regions that request 4 b-jets and 5 b-jets are needed. The signal region corresponds to the criteria of 6 b-jets. A profile likelihood ratio fit is performed over the output score of a Deep Neural Network. The limit on the triple-Higgs boson production is 750 × SM. The 95% C.L. observed intervals for the triple- and quadruple-Higgs boson coupling are, respectively, $-11 < \kappa_3 < 17$ and $-230 < \kappa_4 < 240$.

4. Conclusion

Exploration of the Higgs sector has been updated with respect to previous edition of this conference, with measurement of the Higgs boson width using a novel method of Neural Simulation-Based Inference, improving significantly the sensitivity, update on results of VH and ttH with $H \to bb$ final state, VH with $H \to cc$, and eventually $H \to \tau\tau$. The Higgs boson combination has been interpreted in terms of EFT. Search for double-Higgs boson production establishes an observed limit of 2.9 × SM. Search for triple-Higgs boson production has started, using the 6 b final state. So far, the SM has never been faulted in the Higgs sector. The prospects are for Run 3 which benefits from a higher luminosity than Run 2 with increased energy and novel techniques of machine learning for general selection as well as for tagging primary objects such as b-jets hadrons. Future analyses may outperform the inverse square root luminosity dependence of sensitivity.

REFERENCES

[1] ATLAS Collaboration, *J. Instrum.* **3**, S08003 (2008).

[2] ATLAS Collaboration, arXiv:2412.01548 [hep-ex].

[3] J. Brehmer, G. Louppe, J. Pavez, K. Cranmer, *Proc. Nat. Acad. Sci.* **117**, 5242 (2020).

[4] J. Brehmer, K. Cranmer, G. Louppe, J. Pavez, *Phys. Rev. D* **98**, 052004 (2018).

[5] J. Brehmer, F. Kling, I. Espejo, K. Cranmer, *Comput. Softw. Big Sci.* **4**, 3 (2020).

[6] K. Cranmer, J. Brehmer, G. Louppe, *Proc. Nat. Acad. Sci.* **117**, 30055 (2020).

[7] ATLAS Collaboration (G. Aad *et al.*), *Eur. Phys. J. C* **75**, 335 (2015).
[8] ATLAS Collaboration, arXiv:2410.19611 [hep-ex].
[9] ATLAS Collaboration (G. Aad *et al.*), *Eur. Phys. J. C* **81**, 178 (2021).
[10] ATLAS Collaboration, *Phys. Lett. B* **816**, 136204 (2021).
[11] ATLAS Collaboration (G. Aad *et al.*), *Eur. Phys. J. C* **82**, 717 (2022).
[12] LHC Higgs Cross Section Working Group (J.R. Andersen *et al.*), arXiv:1307.1347 [hep-ph].
[13] LHC Higgs Cross Section Working Group (D. de Florian *et al.*), arXiv:1610.07922 [hep-ph].
[14] ATLAS Collaboration, *Eur. Phys. J. C* **85**, 210 (2025), arXiv:2407.10904 [hep-ex].
[15] ATLAS Collaboration (G. Aad *et al.*), *J. High Energy Phys.* **2025**, 10 (2025), arXiv:2407.16320 [hep-ex].
[16] A. Elagin, P. Murat, A. Pranko, A. Safonov, *Nucl. Instrum. Methods Phys. Res. A* **654**, 481 (2011).
[17] I. Brivio, Y. Jiang, M. Trott, *J. High Energy Phys.* **2017**, 070 (2017).
[18] B. Grzadkowski, M. Iskrzyński, M. Misiak, J. Rosiek, *J. High Energy Phys.* **2010**, 085 (2010).
[19] ATLAS Collaboration (G. Aad *et al.*), *J. High Energy Phys.* **2024**, 097 (2024).
[20] ATLAS Collaboration (G. Aad *et al.*), *J. High Energy Phys.* **2025**, 45 (2025), arXiv:2407.15550 [hep-ex].
[21] ATLAS Collaboration, *Phys. Lett. B* **855**, 138762 (2024).
[22] ATLAS Collaboration (G. Aad *et al.*), *Eur. Phys. J. C* **84**, 78 (2024).
[23] ATLAS Collaboration (G. Aad *et al.*), *Phys. Rev. Lett.* **133**, 101801 (2024).
[24] ATLAS Collaboration, *Phys. Lett. B* **843**, 137745 (2023).
[25] R. Alonso *et al.*, *Phys. Lett. B* **722**, 330 (2013); *Corrigendum ibid.* **726**, 926 (2013).
[26] G. Buchalla, O. Catà, C. Krause, *Nucl. Phys. B* **880**, 552 (2014), *Corrigendum ibid.* **913**, 475 (2016).
[27] ATLAS Collaboration (G. Aad *et al.*), *Phys. Rev. D* **111**, 032006 (2025). arXiv:2411.02040 [hep-ex].